

## A new resonant thermometer for nuclear reactor applications

To cite this article: A A Fathimani and J F W Bell 1978 *J. Phys. E: Sci. Instrum.* **11** 588

View the [article online](#) for updates and enhancements.

### You may also like

- [Two water wheels performance in series for empowerment of irrigation](#)  
Asral, F Huda and M Akbar
- [US firm pursues thorium power](#)  
Alexander Hellemans
- [PLANT GROWTH REGULATOR OF AUXIN CONTENT IN FERMENTED COCONUT WATER WASTE](#)  
Elik Murni Ningtias Ningsih, Sudyono and Frida Dwi Anggraeni

# A new resonant thermometer for nuclear reactor applications

A A Fathimani† and J F W Bell

Department of Electrical Engineering, The University of Aston, Birmingham B4 7PB, UK

Received 5 October 1977, in final form 28 December 1977

**Abstract** An ultrasonic thermometer using the temperature dependence of ultrasonic velocity as the transducing mechanism has been developed for high temperature measurement. Essentially it is a long, thin probe consisting of a magnetostrictive launcher producing longitudinal vibrations in an acoustic line. A resonator which terminates the line constitutes the sensor. By measuring its natural resonant frequency as a function of temperature a calibration of the probe is obtained. A pulse excitation technique is used to drive the resonator after which the oscillations decay exponentially (the decrement) at the natural frequency of the resonator. The control compares this frequency with that of a signal generator to produce an error signal. This is used to make the signal frequency track that of the sensor. Digital aperiodic techniques are used throughout giving a smooth operation over the full range of the instrument. The setting-up procedure for changing a probe is minimal.

## 1 Introduction

The thermometer which was described at the international colloquium on high-temperature in-pile thermometry (Bell *et al* 1974) has been further developed, simplifying the acoustic probe and improving the electronics and automatic control. Further work on probe materials has been carried out and the advantages of ceramic materials, in particular sapphire, over the refractory metals have been quantified.

Physically the probe is of uniform-section rod or strip sufficiently long to enable the magnetostrictive launcher to be located in the cool part of the reactor and the temperature sensor at the point of measurement. The minimum convenient probe diameter is 1.5 mm and the probe must fit loosely into its supports. No protective sheathing is required and, in the case of a strip probe, rapid thermal contact with gas coolant or local thermal radiation is achieved. Acoustically the probe can be considered as an acoustic transmission line terminated by a resonator (the temperature sensor). It

has been analysed extensively as a single resonator (Bell 1968, 1971, 1972), a distributed body with an arbitrary spectrum of resonances (Sharp 1974) and from the point of view of internal friction (Pelmore 1975). In practice a burst of longitudinal oscillations is transmitted up the line and the returned signal, which is separated from the transmission by the time delay on the line, is processed to obtain the resonant frequency. A feature of the current probe design (Seth 1974, Fathimani 1976) is that the resonator is integral with the line, being machined in the form of a tuning fork on the line itself. This avoids the problem of previous designs where the resonator was fixed to the end of the line by a joint which proved unsatisfactory under thermal cycling.

An extensive study of a wide range of refractory materials for the probe identified molybdenum, iridium and tungsten as satisfactory for a number of applications. When attention was directed to ceramic materials, sapphire was found to have numerous advantages, particularly in respect of stability of calibration which remained within  $\pm 2^\circ\text{C}$  after many cycles to  $1800^\circ\text{C}$ . Tungsten and thoriated tungsten (W-2% ThO<sub>2</sub>) were finally selected for a Euratom application.

## 2 The acoustic principle

The analysis of the echo returned from a transmission line terminated by a resonator has been carried out in extreme detail. Figure 1 shows a theoretical computer plot of an echo for the resonant condition, and an oscilloscope plot of a similar echo with a diagram identifying salient features.

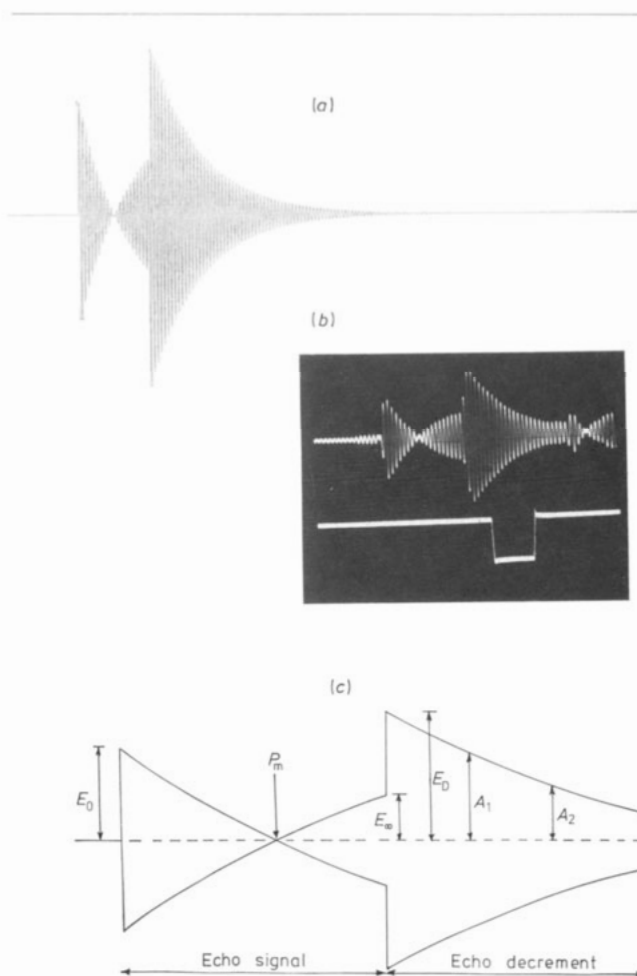


**Figure 1** (a) Theoretical computer plot of an echo for the resonance condition. (b) Real echo pattern established on the CRO. (c) Diagram identifying the echo specifications.

† Present address: Nuclear Technology Department, Institute of Nuclear Science and Technology, Tehran University, PO Box 2989, Tehran, Iran.

The waveforms represent the reflected signal delivered by the magnetostrictive transducer a substantial time after this transducer has delivered a burst of oscillations to the line (see upper part of figure 4). These have a rectangular envelope which is equal in length to that of the echo signal as shown in figure 1. The frequency within the triangular envelope of the echo signal is that of the transmitted signal. The shape of these envelopes is due to the interaction between the transmitted signal and the forced oscillation in the resonator, both at the original transmitted frequency.

The signal changes exponentially starting with an amplitude  $E_0$ , falling to zero after  $P_m$  oscillations and then rising towards a steady state value of  $E_\infty$ . At the end of the signal the energy stored in the resonator leaks back down the line. This is known as the echo decrement. It is a fundamental feature of the echo decrement of a resonator that it is at the natural resonant frequency of the resonator, irrespective of the drive frequency. The echo waveform goes sharply to zero at  $P_m$  when the transmitted frequency and the resonator frequency are adjusted to be equal. At this frequency there is then a sharp reversal of phase as the echo waveform goes through zero. The amplitude of the echo decrement, of course, falls off as the drive frequency is tuned away from the resonator frequency, and the echo waveform will not pass through a sharp zero, but rather through a region of minimum amplitude in which the phase is in quadrature with the phase at earlier or later times. The decrement frequency is therefore measured with high accuracy in the signal processing.

The exponent of the echo decrement is the same as that of the echo signal. The form is given by

$$A_n = A_0 \exp(-\pi n/Q) \quad (1)$$

$A_n$  is the amplitude after  $n$  oscillations and is expressed in terms of  $Q$ .

In the absence of internal friction,  $E_\infty = E_0$  and the energy loss associated with the  $Q$  is due to the coupling between the line and the resonator. It is related to  $P_m$  by

$$P_m = Q_c \times 0.22 \quad (2)$$

In the presence of internal friction, a material property which rises to large values at high temperatures,  $E_\infty$  falls. It reaches zero when the internal friction loss is equal to the line-coupling loss. This feature represents the useful temperature limit of the material. The sensor is machined

to make  $P_m$  about 11 at room temperature ( $Q_c = 50$ ). A lower  $P_m$  makes the  $Q$  too low to allow a sufficient sample of the decrement to be obtained. These parameters enable platinum (melting point MP 1650°C) to be used to 1250°C, iridium (MP 2400°C) to 1800°C and sapphire (MP 2050°C) to 1950°C. Equation (3) gives the  $E_\infty/E_0$  ratio in terms of the material and coupling  $Q$  factors:

$$\frac{E_\infty}{E_0} = \frac{Q_c - Q_m}{Q_c + Q_m} \quad (3)$$

When  $Q_m \gg Q_c$  then  $E_\infty/E_0 = -1$ , indicating a phase reversal and a null; when  $Q_m = Q_c$ ,  $E_\infty$  is asymptotically zero and when  $Q_m < Q_c$  there is no crossover and the decrement is small and cannot be processed to the accuracy required for thermometry.

### 3 Probe acoustics

The sensor is in the form of a tuning fork which is integral with the line and is machined precisely at the end of the acoustic line. It can be used on a rod or strip. Figure 2 shows the sectional diagram of the new design of integral tuning fork, developed by Fathimani (1976). The tines are formed by the longitudinal slot. The width of the neck ( $W_n$ ) has the effect of coupling the longitudinal waves to the flexural vibration of the fork. The investigations have shown that the minimum coupling  $Q$  between the resonator and the line will be achieved at the quarter-wavelength of the resonator. The mechanism can be visualised by considering the alternating longitudinal forces on the axis of the fork. These exert a mechanical moment on each tine driving both of them into clamped-free flexural vibrations. The characteristic dynamic balance of the fork occurs because of the reverse phase vibration of the tines. The only design variables available to give the required frequency and coupling are the tine length ( $l$ ) and the position and depth of the resonator neck ( $N_t$ ). But the width of the neck ( $W_n$ ) of the resonator is the most effective design parameter governing the tightness of the coupling in conjunction with low frequencies. The frequency of the clamped-free bar is related to  $c$ , the longitudinal velocity of sound in the material, the length  $l$  and the width  $w$  of the tines by

$$f \propto cw/l^2 \quad (4)$$

Once a geometrical form is obtained an increase of scale lowers the frequency proportionately but the coupling is

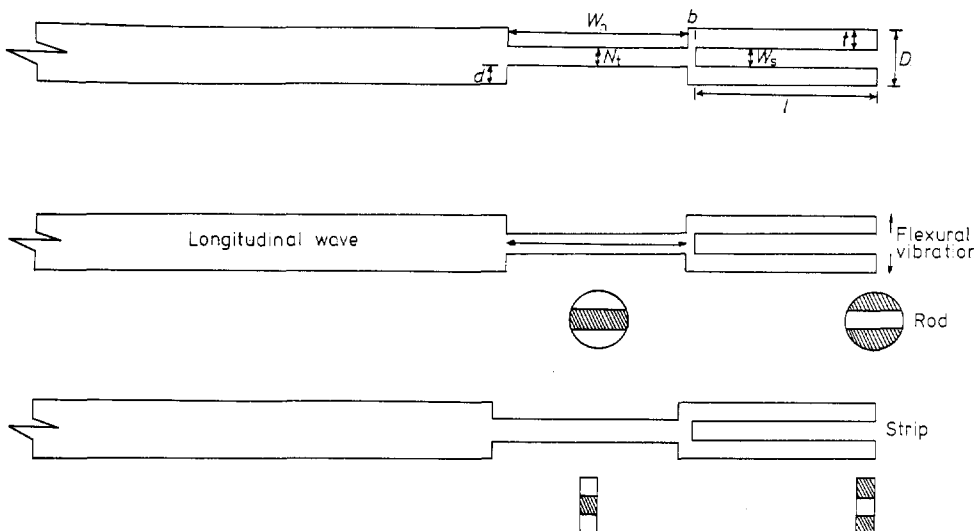


Figure 2 Sectional diagram of the new design of integral tuning fork based on 1.5 mm rod or strip.  $D$ , Diameter of the rod;  $l$ , length of the tine;  $b$ , length of the base;  $t$ , thickness of the tine;  $W_s$ , width of the longitudinal slot;  $W_n$ , width of the neck = quarter-wavelength;  $d$ , depth of the neck;  $N_t$ , neck thickness.

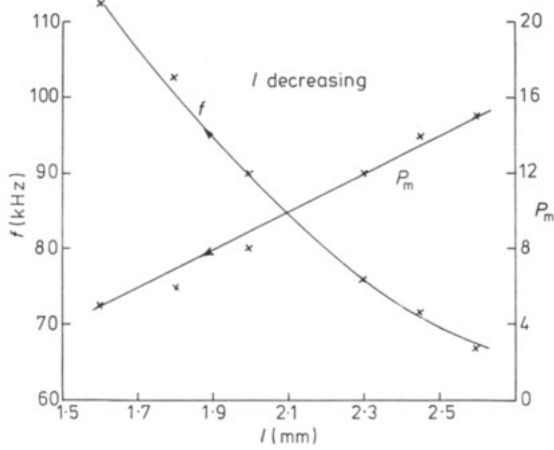


Figure 3 Effect of the tine length on the frequency and  $Q$  factor in terms of number of oscillations to crossover ( $P_m$ ) of an integral line resonator.

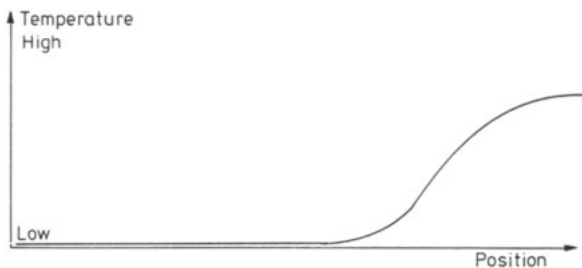
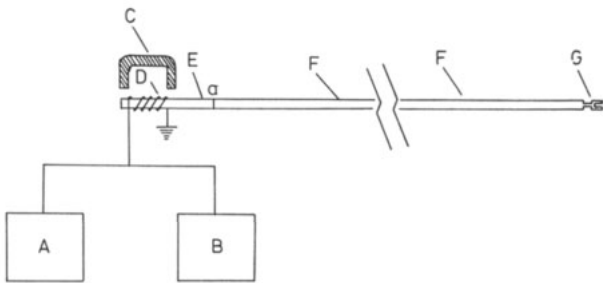


Figure 4 General form of the line and temperature profile of the system. A, electronic system; B, CRO; C, magnet; D, launcher and receiver coil; E, transducer rod (Permandure); F, lead-in rod (acoustic transmission line); G, resonator.

unchanged. Some difficulty was experienced in obtaining sufficient coupling while retaining a robust design. Figure 3 shows how, for a given design, reduction in tine length increases the frequency and coupling, represented by a fall in the number of oscillations to crossover. Even with high-velocity ceramic materials such as sapphire the design gives a conveniently low frequency of about 150 kHz on a 3 mm rod.

Figure 4 shows the general form of the line. Acoustic matching requires that the acoustic impedance  $\rho c A$  (where  $A$  is the area of cross section and  $\rho$  the density) is constant in all parts of the line. There is usually only one joint in the line and that is at the magnetostrictive transducer side (point a). Spurious signals from joint and supports are a source of error if they overlap the echo. Acoustic matching techniques for making joints between lines of various cross sections and materials (Seth 1974) result in obtaining a

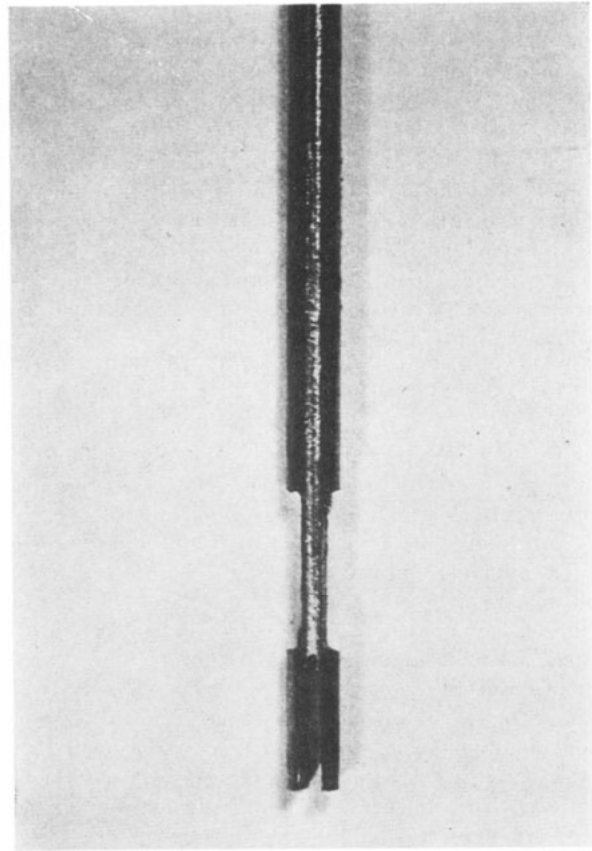


Figure 5 Photograph of one of the new 1.5 mm integral tuning forks, cut on the thoriated tungsten rod for the experimental work.

good acoustic matching with good mechanical strength and hence reduction of the residual echoes.

As the waves occupy the whole cross section of the line, the effect of supports decreases with increase in line diameter. It is therefore of advantage to make use of all the space available for the probe by using as large a line diameter as possible. A high  $\rho c$  is equally advantageous. In a nuclear reactor it is recommended making the whole length of the acoustic transmission line from molybdenum metal which has a very high  $\rho c$  and a low capture cross section for neutrons.

In all of the experiments which were performed to calibrate a thoriated tungsten probe for the 'Petten' reactor, a sample rod (of 1.5 mm  $\times$  200 cm, tungsten-2% thoria) was used which had a precisely machined tuning fork at one end (figure 5) and which was silver-brazed to a 6 cm launcher at the other end.

#### 4 Electronic circuits

The function of the electronics is to maintain a signal generator at the same frequency as that of the sensor. The essence of the problem is that the sensor is at the remote end of the probe, a large number of wavelengths away, and this excludes the use of a conventional resonator-maintained oscillator. Figure 6 shows the system used. The resonator period  $D$  is extracted from the echo decrement and compared to the signal generator period  $S$  giving an error voltage. This is reduced to zero by the control loop which is a second-order system. The echo is identified, five or ten specific oscillations of the decrement are sampled and their duration compared with high precision to that of five or ten signal oscillations.

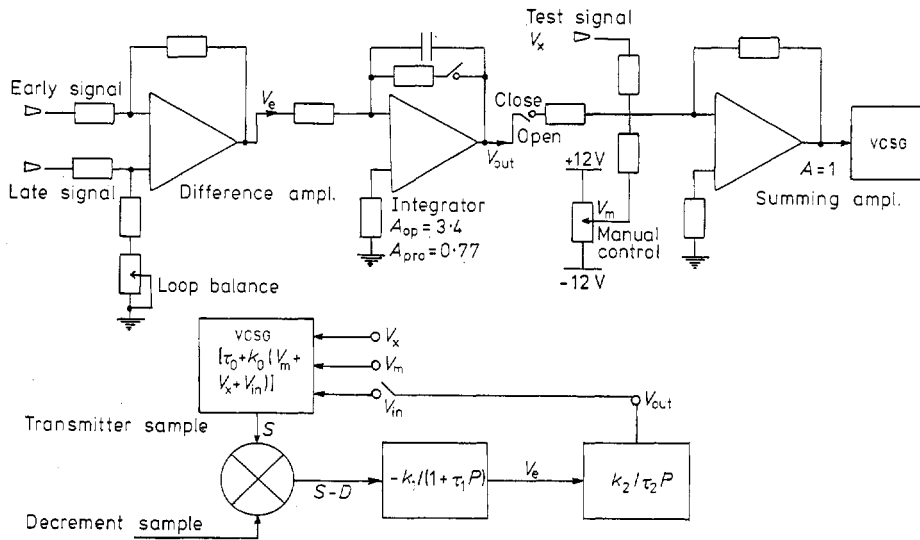


Figure 6 Control system illustrated in two forms, functional and block diagram. vcsg, voltage-controlled signal generator.

The system must operate smoothly over a frequency range of about 40%, the maximum working range of most probe materials. A discontinuity in performance, such as a shift in the group of cycles in the decrement selected for measurement, can result in a small step change in output reading. Being completely automatic the system must find resonance from either extreme of frequency. Digital techniques were used as extensively as possible. Typically the sinusoidal echo signal is squared using a zero crossing detector and then processing digitally. Also when required, signal delays are obtained in terms of number of pulses rather than as a fixed time interval. The facility to test the various elements of the system was incorporated in the design and this enabled sources of noise and second-order errors to be identified. The technology is based on TTL integrated circuits and makes minimal use of discrete components and analogue devices. The control loop is, however, of the conventional analogue type.

5 Signal generator

The signal generator is used to produce a number of waveforms (figure 7). It is essentially a free-running multivibrator

which, with associated multiplexing circuits, can be switched on and off via four independent channels each having an input and an output (figure 8). On receipt of a trigger pulse the multivibrator will run for the number of cycles designated by the channel, the signal appearing only at the one channel output. By operation of the multivibrator at twice the required signal frequency and dividing by two, two phases are available, each of equal mark:space ratio, enabling delay steps of half a cycle to be obtained as required. The multivibrator consists of two cross-coupled TTL monostables using external timing resistors. Being an aperiodic oscillator it can be switched on and off very precisely without time delay or transient. This feature is used extensively. Voltage control of frequency is obtained by additional timing resistors driven from the output of a DC amplifier. The values were chosen to give a frequency coverage of  $\pm 50\%$  about a centre value. The random frequency changes from second to second are of the order of 1 in  $10^5$ . This stability is well within the target performance of the instrument (1 in  $10^4$ ) where the control loop and readout act in a fraction of a second. On open-loop operation, long-term drift arises from the  $0.6\% K^{-1}$  temperature coefficient and the  $0.05\% mV^{-1}$  change of chip voltage.

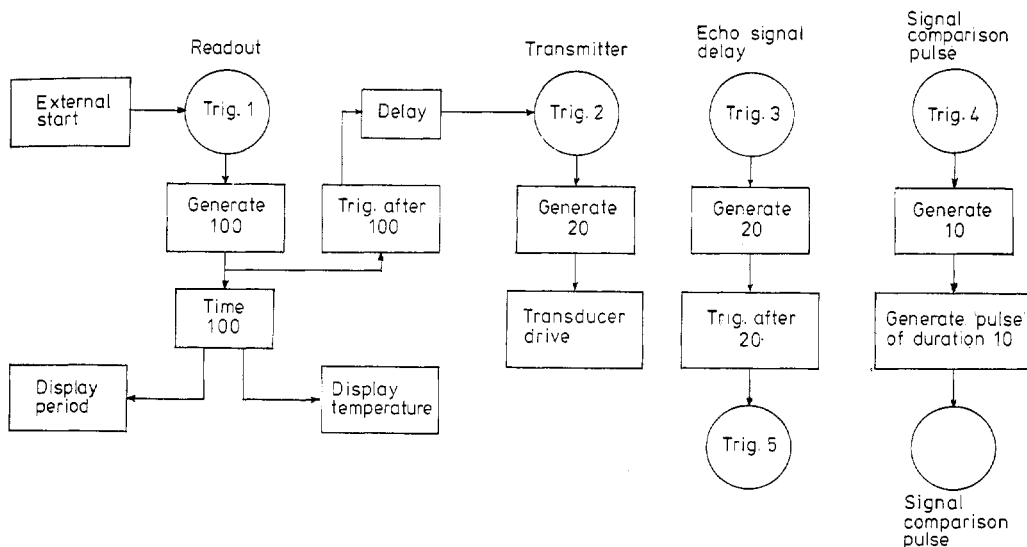


Figure 7 Functional diagram of the signal generator which is used to produce a number of waveforms.

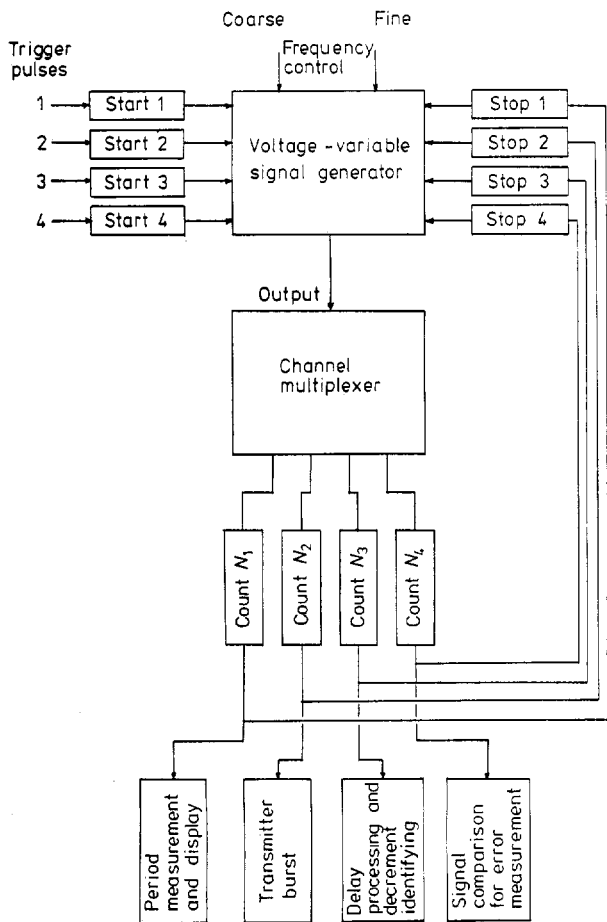


Figure 8 Channel multiplexer and operating cycles of the electronic system.

6 Operating cycle

In the cycle of operations (figures 7, 8 and 9) a starting pulse (trig. 1) operates the readout channel. This enables the time for 100 oscillations to be measured. A 10 MHz crystal clock gives a readout of  $\pm 1$  in  $10^4$  at 100 kHz and better than this at lower frequencies. Other circuits, preset for a particular probe calibration, give a direct readout of temperature.

The readout is followed (trig. 2) by a burst of 20 oscillations which operates a complementary pair of power transistors driving the magnetostrictive transducer. The harmonics present in the square wave are greatly reduced by the selectivity of the transducer and are not observable in the echo decrement.

The next signal is initiated by trig. 3 which occurs at a zero crossing near the beginning of the returned echo signal. Trig. 5 is produced 20 periods later. It is after the beginning of the decrement but because of the finite bandwidth of the transducer there is a transient of a few oscillations before the decrement is effectively established. There is therefore a further delay of five echo cycles before trig. 4, which again is synchronous with a zero crossing, initiates the signal comparison circuit. The comparison pulse generated lasts for precisely ten signal periods but is delayed by half a period.

The operating cycle is now complete and the signal generator awaits the arrival of the next trig. 1. This interval is made just sufficiently long to allow reverberations on the probe to die down. Of course the shorter the interval the more efficient will be the control loop. The echo return is of the order of 1 V peak-to-peak and has no significant acoustic or electronic noise. An integrated circuit voltage comparator giving a TTL-compatible pulse output with a sensitivity of a fraction of a millivolt is used to interface the analogue-to-digital signals. The echo signal drives two comparators: one, unbiased and therefore acting as a zero crossing detector, produces square waves; the other, with a fraction of a volt bias, detects the arrival of the echo signal. Producing trigger 3 the operation of the comparators can be inhibited by a TTL pulse and they are suppressed during the signal transmission. The bias must be selected to cover the same part of the echo signal over the full temperature range of the probe.

7 Error measurement

As indicated in the echo-processing diagram the signals are then processed to give the decrement comparison pulse which lasts for ten decrement periods (figures 10 and 11). It starts half a period before and extends beyond the signal comparison pulse. These two pulses are the basis of producing the error signal which is proportional to the difference between decrement and signal period. The error measurement is a determining factor in the overall accuracy of the instrument. It is obtained from the signal and decrement comparison pulses (figure 12). Let each be of  $n$  cycles' duration and the signal pulse be delayed by  $D/2$ . Two short pulses are derived from them, the early and late overlap pulses of duration  $D/2$  and  $(D/2) + n(S - D)$  respectively. The late pulse can be numerically negative when  $S < D/(1 + 1/2n)$  but no pulse is generated for this condition. Thus as  $S$  is increased from a small value the late pulse width remains at zero until  $S = D/(1 + 1/2n)$ , after which it increases linearly with  $S - D$ , the pulses being equal when  $S = D$  and the error is zero (figure 13). The pulse durations are converted to voltages by two integrators and subtracted to give the error signal (figure 11). The storage time constant of the integrators

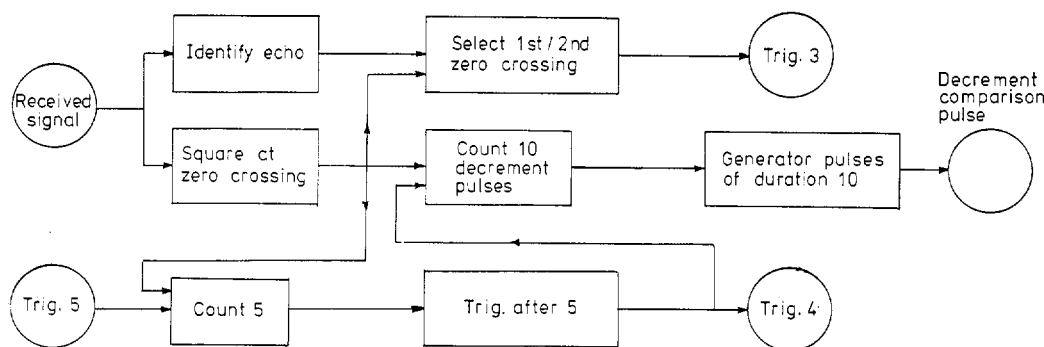


Figure 9 Functional diagram of the echo-processing circuit.

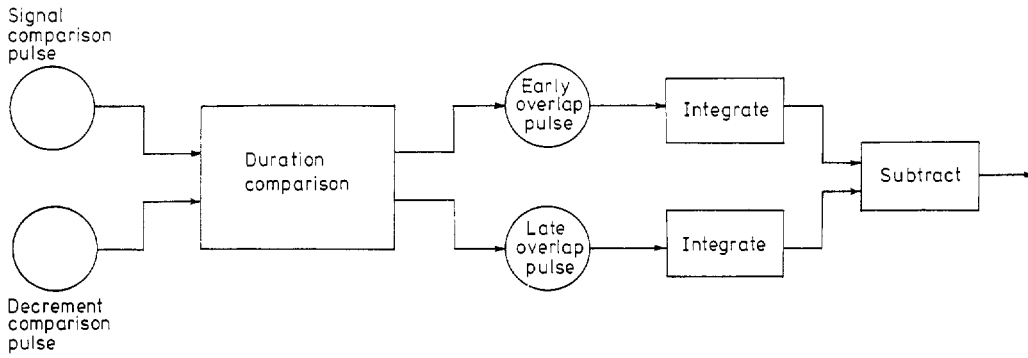


Figure 10 Functional diagram of the error measurement circuit.

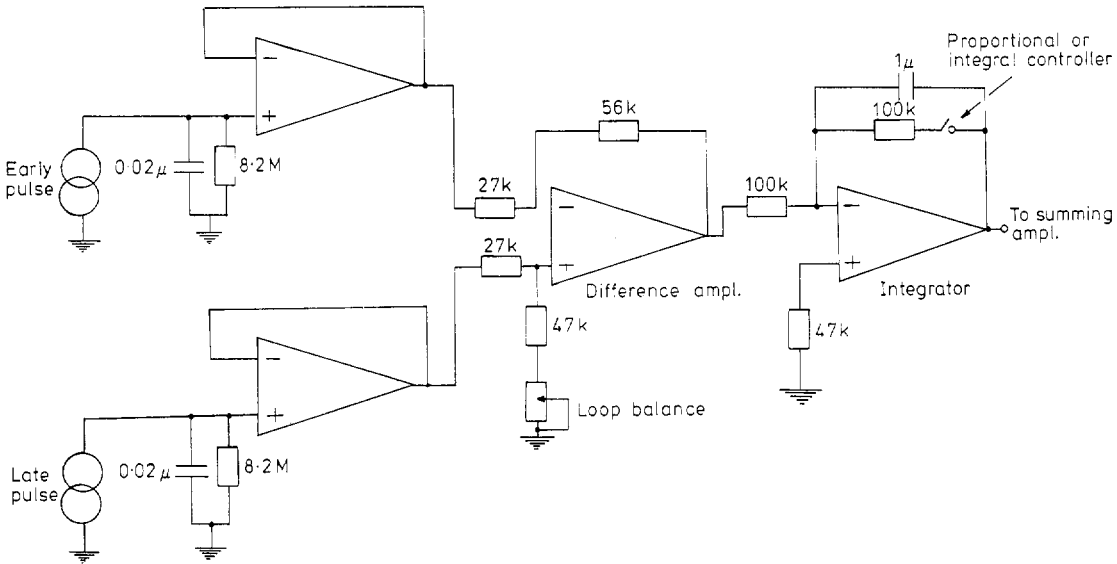


Figure 11 Circuit details of the error measurement.

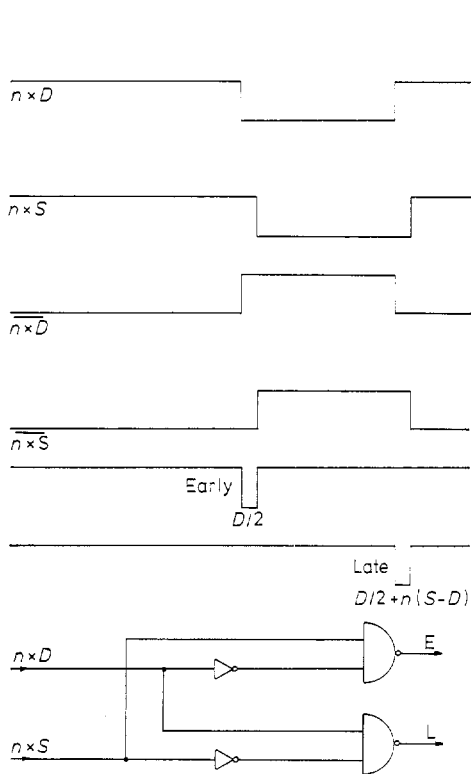


Figure 12 Waveform of the sampling comparison.

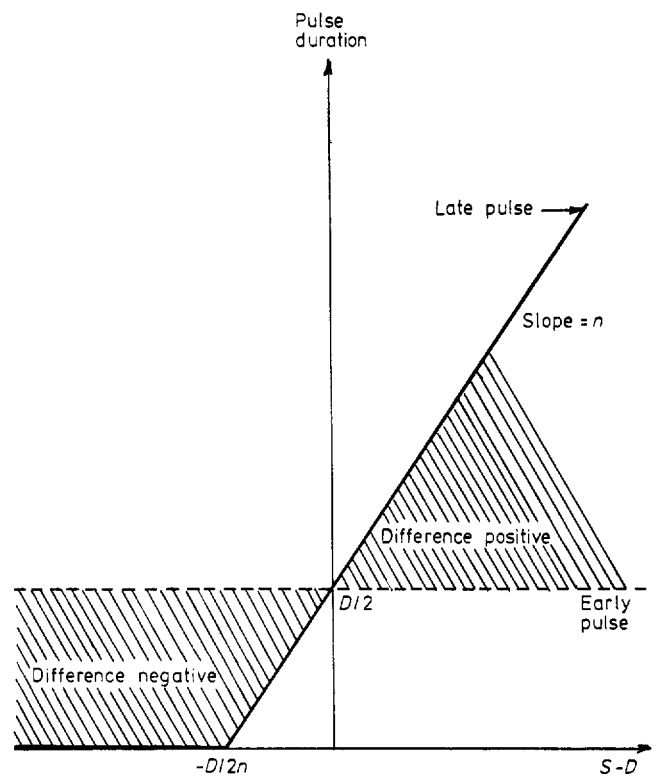
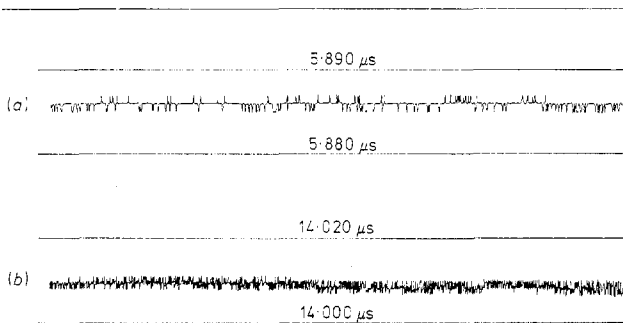


Figure 13 Analytical diagram for the error measurement system.

is four or five times the cycle time of the instrument and constitutes the major signal delay in the control loop. So long as there is a detectable decrement the polarity of the error signal will give the true sense of  $S - D$ . In the absence of a decrement the control, which is second-order and consequently incorporates an integrator, will drive the signal generator to a high- or low-frequency extreme. In practice, once established, control is not lost even with very rapid temperature cycling. An alarm could however be incorporated by monitoring the decrement signal.

The error measurement (figure 11) is a determining component of the sensitivity of the control system. In terms of a decrement period, for measuring accuracy of 1 in  $10^4$  and a  $10 \mu\text{s}$  period, a sample of ten oscillations requires a 10 ns resolution. The initial sample of  $5 \mu\text{s}$  gives 5 V output and the measuring accuracy required is therefore 5 mV. Noise in the output originates from intrinsic electronic noise, pulse width or edge noise and data noise arising from genuine temperature fluctuations of the sensor. If the early pulse ( $D/2$ ) is applied to both channels, only intrinsic noise will appear at the difference amplifier output. Similarly pulse width noise can be identified by keeping the sensor at constant temperature. Figure 14 summarises these tests and establishes that fluctuations in period greater than about 1 in 5000 arise from instrumentation noise. The main source of noise proved to be in the conversion of the sinusoidal decrement to square waves by the zero crossing detector.



**Figure 14** Recorder plot showing the long-term stability of the overall instrument performance. (a) Period fluctuation due to the data noise for sapphire probe: 2 parts in 5000, PRF = 1.25 Hz, time base = 1 min in<sup>-1</sup>. (b) Period fluctuation (instrumentation) noise for iridium probe: 4 parts in 14 000, PRF = 1.25 Hz, time base = 1 min in<sup>-1</sup>.

### 8 The control system

The function of the control is to make the signal generator period follow the variations in decrement period with the temperature (figure 6). The period  $S$  of the voltage-controlled signal generator has three control inputs:  $V_m$  from the manual potentiometer,  $V_{in}$  which is zero until the feedback loop is closed and  $V_x$  which is available for performance tests. These voltages are applied through equal resistors to a summing point. Equation (5) expresses the relationship:

$$S = \tau_0 + k_0(V_{in} + V_m + V_x). \quad (5)$$

$\tau_0$  is preselected to be in the mid-range of the probe in use and  $k_0$  enables  $S$  to be varied over about  $\pm 50\%$  for  $\pm 10$  V input, the dynamic range of the amplifiers.

The error measurement averages the difference between  $S$  and  $D$  over about five recurrence cycles. This averaging involves a significant delay which is represented by the denominator in the error voltage (equation (6)). In the steady state the denominator is unity and in the case of a step in

$S$  or  $D$ ,  $V_e$  approaches the steady state value exponentially, following the function  $1 - \exp(-t/\tau_1)$ .

$$V_e = \frac{k_1}{1 + \tau_1 P} (S - D). \quad (6)$$

On closing the loop the error signal can be fed back to the input either via a unity-gain amplifier giving proportional control or via an integrator giving integral control. The latter is a second-order system controlling down to zero error.

The overall open-loop transfer function for integral control is given by equation (7). On proportional control the Laplace factor becomes  $k_1/(1 + \tau_1 P)$ , and

$$V_{out} = \frac{V_e}{\tau_2 P} = \frac{k_1/\tau_2}{P(1 + \tau_1 P)} [\tau_0 + k_0(V_{in} + V_m + V_e - D)]. \quad (7)$$

When the loop is closed with negative feedback then  $V_{in} = V_{out}$  and the dynamic performance can be found by differentiating equation (5) with respect to  $V_x$ , giving

$$\frac{\partial V_{out}}{\partial V_x} = \frac{k_0 k_1 / \tau_2}{P(1 + \tau_1 P)} \left( 1 - \frac{\partial V_{out}}{\partial V_x} \right). \quad (8)$$

Equation (9) gives the standard form for unity negative feedback, where

$$A = \frac{k_0 k_1 / \tau_1 \tau_2}{P(P + 1/\tau_1)} = \frac{k}{P(P + 1/\tau_1)},$$

$$\frac{\partial V_{out}}{\partial V_x} = \frac{1}{1 + 1/A} = \frac{k}{P^2 + (1/\tau_1)P + k}. \quad (9)$$

The steady state performance is shown in figure 15. The unity-gain amplifier (making  $V_{out} = V_e$ ) is used to obtain the open-loop and proportional characteristics. The slopes are 3.4, the loop gain  $k_0 k_1$  and 0.77 – equal to  $k_0 k_1 / (1 + k_0 k_1)$  – respectively. On ‘integration’, the integrator replaces the unity-gain amplifier and  $V_e = 0$ . This requires  $\partial V_{out} = -\partial V_x$  and  $S = D$ .

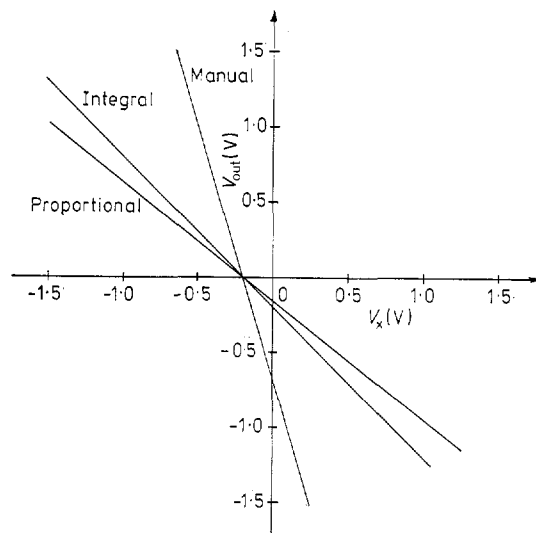


**Figure 15** Relationship between  $V_{out}$  and  $V_x$  for three conditions: the open loop, the closed loop proportional and the closed loop on integrate. On integrate, the slope is unity as the feedback voltage nullifies  $V_x$ . The slope on open loop is the open-loop gain  $A$  ( $= 3.4$ ) and on proportional is  $A/(1 + A) = 0.77$ . It will be noted that, for a particular value of  $V_x$ ,  $V_{out}$  is zero for all three conditions.

The dynamic response was examined on integral control which is the normal operating mode of the instrument. A step input  $V_x$  was applied and the responses of  $V_{out}$  and  $S$  were displayed as functions of time. Two values of the gain were used, 3.4 when the system is overdamped and 34 when it is underdamped. When step  $V_x$  applies,  $V_{out}$  goes to a new value (equal to  $-V_x$ ) and  $S$  is returned to its original value. The discrete steps correspond to error samples taken every recurrence cycle. The smoothness of static and dynamic characteristics establishes the stability of operation of all the various circuit units.

**9 Probe materials and instrument performance**

Iridium, available commercially as an alloy with a small percentage of platinum to make it machinable, has a performance typical of all the refractory metals. A probe was prepared from a strip 0.025 cm x 0.45 cm x 25.4 cm. It was calibrated by heating it in steps of temperature in a coal-gas-oxygen flame, the temperature being measured optically. Figure 16 shows the steps as a function of time.

Two deficiencies were at once apparent: the internal frictions associated with the grain boundaries of the polycrystalline material became excessive above 1700°C and changes due to grain growth caused a calibration drift with thermal cycling. Figure 17 gives an automatic calibration curve to 1000°C, indicating the performance of the electronics. The X axis shows temperature obtained from a thermocouple voltage and the Y displacement is proportional to period, obtained from a digital-to-analogue converter. The cycle, which lasted about 3 h, shows the close agreement between heating and cooling curves. The fluctuations are the instrumentation noise; the ultimate limit of the instrument (see figure 18) shows two cycles of heating in a gas flame to the limit of the probe. Again smooth curves are obtained showing the stability of the instrument and the smoothness in following rapid temperature changes.

The single-crystal form of alumina, sapphire, is readily available and 3 mm rods, 25.4 cm long were used. The internal friction proved to be very small and good performance to within a hundred degrees or so of the melting point (2050°C) was obtained. Figure 19 gives an excellent indication of performance. The probe temperature was held constant, as far as possible, in a gas flame and the period was recorded continuously over 15 min runs. The figure shows the performance to be as good at 1900°C as at low

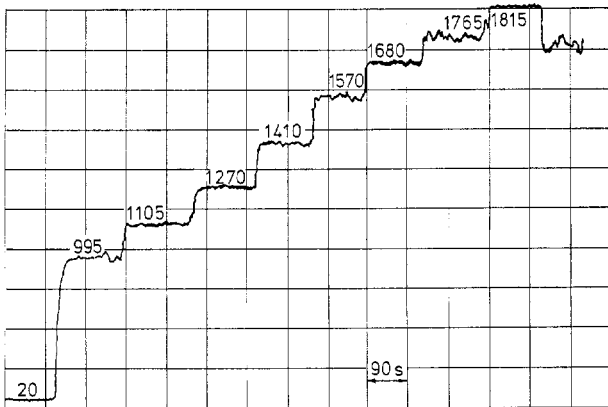


**Figure 16** Recorder plot of the various step positions of an iridium probe during heating in a blowtorch flame. The fluctuation is due to instability of the flame temperature. Temperatures on the steps are in °C.

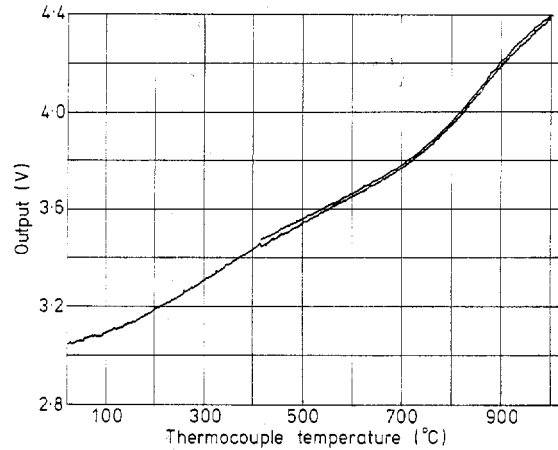


**Figure 17** Automatic calibration of an iridium ultrasonic probe against a thermocouple between 0 and 1000°C. The plot shows the close agreement between heating and cooling curves.

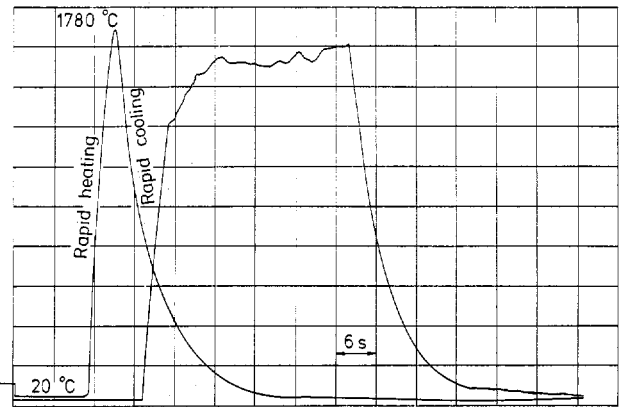


**Figure 18** Plot of two cycles of heating in a gas flame to the limit of the iridium probe. Smooth curves are obtained demonstrating the stability of the instrument and the smoothness in following a very rapid temperature change.

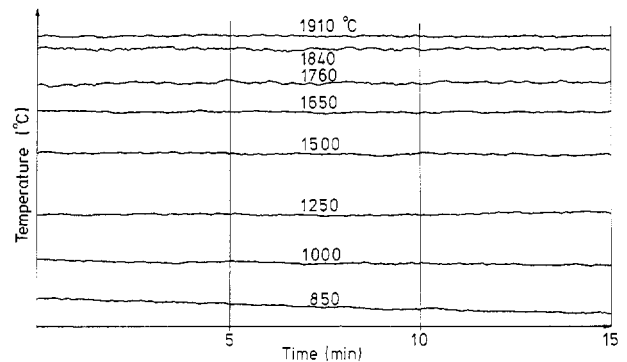


**Figure 19** Temperature stability of the sapphire ultrasonic probe in a blowtorch flame. The figure gives an excellent indication of the system performance. The probe temperature was held constant, as far as possible, in a gas flame and the period was recorded continuously over 15 min runs. The figure shows the performance to be as good at 1900°C as at low temperature.

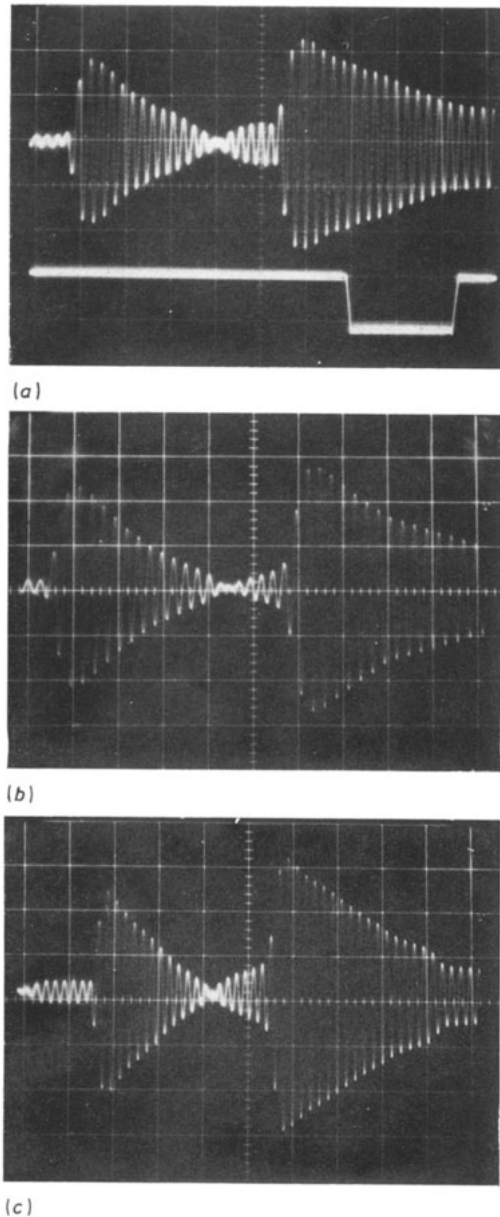


**Figure 20** Corresponding echoes over the temperature range for the sapphire ultrasonic probe. The good crossover at 1850°C will be noted. In all cases,  $P_m = 13$  and sensitivity = 0.05 V cm<sup>-1</sup>. (a) At 20°C, frequency 169.80 kHz. (b) 950°C, 158.80 kHz. (c) 1850°C, 150.6 kHz.

temperature. Measurements over a number of thermal cycles established a very high stability of calibration amounting to  $\pm 2^\circ\text{C}$ . Figure 20 shows the corresponding echoes over the temperature range. The clear crossover at 1850°C will be noted.

### 10 Application

As indicated before, the essential feature of the instrument is the automatic precision tracking of the electronic drive signal generator with the natural resonant frequency of the mechanical resonator under investigation. This makes use of a specially designed resonant transducer, the frequency of which can be made sensitive to the parameter required, typically temperature, force, pressure or various fluid properties. The use of temperature has been described and applies to nuclear reactors, liquid metal systems and other applications where the environment prevents the use of conventional materials and techniques (Fathimani 1976).

The apparatus has also been used for the measurement of the mechanical properties of isotropic and orthotropic materials. It is quite suitable for measuring the Young modulus and Poisson ratio as functions of temperature. Internal friction measurement of refractory metals in the frequency range 10–500 kHz have been investigated extensively (Pelmore 1975).

### References

- Bell J F W 1957 The velocity of sound in materials at high temperatures  
*Phil. Mag.* **2** 1113–20
- Bell J F W 1958 Dynamic and static elasticities of solids  
*Nature* **181** 1330
- Bell J F W and Doyle B P 1964 Sound pulses in thin non-uniform rods  
*Ultrasonics* **2** 39–42
- Bell J F W *et al* 1966 An instrument for the measurement of acoustic pulse velocity and attenuation in a solid probe  
*J. Sci. Instrum.* **43** 28–31
- Bell J F W 1968 A solid acoustic thermometer  
*Ultrasonics* **6** 11–14
- Bell J F W 1971 Ultrasonic thermometry using resonance techniques  
*Proc. 5th Symp. on Temperature, Washington DC*
- Bell J F W 1972 *US Patent No.* 3 633 423
- Bell J F W, Noble A E and Seth T N 1973 Graphical displays of acoustic properties of solids  
*Ultrasonics* **11** 178–81
- Bell J F W, Fathimani A A and Seth T N 1974 An ultrasonic thermometer using a resonant sensor  
*Int. Colloq. on High Temperature In-pile Thermometry, JRC Petten, The Netherlands* (UKAEA and CEC) 1975 EUR 5395
- Bell J F W, Johnson A C and Sharp J C K 1975 Pulse-echo method of investigating the properties of mechanical resonators  
*J. Acoust. Soc. Am.* **57** 1085–93
- Fathimani A A 1976 The automation of resonant thermometer probe measurements  
*PhD Thesis* University of Aston in Birmingham
- Pelmore J M 1975 Internal friction and high temperature measurement on refractory materials  
*PhD Thesis* University of Aston in Birmingham
- Seth T N 1974 Ultrasonic pyrometer for industrial applications  
*PhD Thesis* University of Aston in Birmingham
- Sharp J C K 1974 A theoretical and experimental investigation in the spectra of selected resonators  
*PhD Thesis* University of Aston in Birmingham